NANO EXPRESS

OPEN ACCESS

RECEIVED
9 August 2021

REVISED
11 June 2022

ACCEPTED FOR PUBLICATION
29 June 2022

PUBLISHED
6 July 2022

PAPER

Probing into crystallography and morphology properties of MoS_2 nanoflowers synthesized via temperature dependent hydrothermal method

Naveen Kumar[1], Piyush Siroha[2], Hari Shankar[3], Davender Singh[4], Yashpal Sharma[5], Rajesh Kumar[1], Ramovatar[2], Navneet Yadav[6], Kajal Kumar Dey[7], Hitesh Borkar[8] and Jitendra Gangwar[4,*]

[1] Department of Physics, Panjab University, Chandigarh, 160014, India
[2] Department of Physics and Astrophysics, Central University of Haryana, Mahendergarh, Haryana, 123031, India
[3] Indian Institute of Remote Sensing, ISRO, Dehradun, 248001, India
[4] Department of Physics, RPS Degree College, Balana, Mahendergarh, Haryana, 123029, India
[5] Department of Chemistry, RPS Degree College, Balana, Mahendergarh, Haryana, 123029, India
[6] Department of Physics, University of Allahabad, Allahabad, Uttar Pradesh, 211002, India
[7] Centre for Nanoscience and Technology, Prof. Rajendra Singh (Rajju Bhaiya) Institute of Physical Sciences for Study and Research, V.B.S. Purvanchal University, Jaunpur, Uttar Pradesh, 222003, India
[8] Department of Physics, National Institute of Technology, Warangal, Telangana, 506004, India
* Author to whom any correspondence should be addressed.

E-mail: njitendrag127@gmail.com

Keywords: MoS_2, nanostructures, hydrothermal synthesis, XRD, FESEM, VESTA

Supplementary material for this article is available online

Abstract

This paper reports the formation of flower-like hierarchical molybdenum disulfide (MoS_2) nanoparticles following a simple one-step hydrothermal process with varying temperatures (200 °C and 220 °C). The as-synthesized particles were examined crystallographically by X-ray diffraction (XRD) method which revealed the formation of hexagonal MoS_2 (2H-MoS_2) and that the crystallite size of the particles increased with increasing hydrothermal temperature. Surface morphological characteristics of the particles were investigated by a field emission scanning electron microscope (FESEM) and interesting details were revealed such as the rounded 3D flower-like microstructure of the MoS_2 particles and the petals of the flowers were composed of platelets built up by stacked-up MoS_2 nanosheets. With the increase in hydrothermal temperature, the interlayer spacing of stacked layers of intense (002) plane is slightly decreased although the crystallinity of the material is improved. Both diameter and thickness of the nanoflowers and the nanoplatelets increased twice with increasing the temperatures. A visual crystallographic perspective was presented through simulation of 3D wireframe unit cell associated with the individual lattice planes as observed in the XRD pattern of the samples. In addition, a plausible growth mechanism is proposed for the formation of the obtained MoS_2 nanoflowers on the basis of experimental observations and analysis.

1. Introduction

Both the preparation and property studies of novel two-dimensional (2D) and/or three-dimensional (3D) nanostructured materials based on metal chalcogenides such as metal-oxides, -sulfides, -selenides, -nitrides with controlled morphology have attracted enormous interest that has steadily grown worldwide because of their exotic properties that are important for various innovative applications [1–12]. In recent years, intensive research has been devoted to producing high-quality 2D and 3D metal sulfide (CoS_2, FeS_2, MoS_2, NiS_2, SnS_2, and WS_2) nanostructures of various morphologies e.g. nanoparticles, nanoflowers, nanosheets, nanospheres and nanolamellar morphology [2, 6, 13–18]. Among the widely known metal sulfides, molybdenum disulfide (MoS_2) is a naturally occurring, well-defined two-dimensional (2D) layered material that has been reported to be an excellent material capable of various

applications owing to its exceptional structural, morphological, optical, thermal, electrical, mechanical, electrochemical, electronic and many other physicochemical properties [6, 15–20]. Due to its layered morphology and tunable direct bandgap, nanostructured MoS_2 has found potential as anode materials in lithium/sodium storage [16, 21, 22], as a catalyst in electrocatalytic reactions [2, 14, 18, 23, 24], in electronics [17, 20, 25], photocatalysis [26, 27], enzymatic reactions [28], antibacterial [29], sensing [27], and photoelectrochemistry [30] etc. Most if not all of these above-mentioned applications depend, to a large extent, on the surface-morphological characteristics of the particles which would dictate essential properties like specific surface area, crystallinity, ability to engage defects etc.

Various hierarchical MoS_2 nanomaterials with different morphologies including 2D tubes-, plates-, ribbons-, sheets-like morphology, and 3D particles-, flakes-, porous-, flowers-like morphology have been obtained via a variety of synthesis procedures; both chemical and/or physical [1, 2, 13, 14, 16–19, 21, 24, 31–35]. MoS_2 flower-like nanostructures have recently gained wide traction due to their unique structural characteristics [16, 21, 24, 27, 36]. The synthesis method usually plays a crucial role in obtaining the desired morphology and related physicochemical characteristics which would be suitable for specific industrial and engineering applications [23, 25]. Zhao *et al* summarized the diverse synthetic approaches, phase, and electronic band structures of metastable MoS_2 [15]. For the synthesis of flower-like MoS_2 morphology, hydrothermal has usually been the method of choice [16–18, 21, 24, 36]. Hu *et al* synthesized MoS_2 nanoflowers by a hydrothermal method followed by freeze-drying [16]. Lu *et al* used a simple hydrothermal method via altering reaction temperatures to produce MoS_2 nanoflowers consisting of nanosheets to be explored as high-performance lithium-ion battery anodes [21]. Wang *et al* prepared amorphous MoS_2 nanoflowers via hydrothermal synthetic routes and discussed their performance in hydrogen evolution reaction (HER) [24]. Zhang *et al* managed to synthesize synthesized 3D flower-like MoS_2 microspheres via a simple hydrothermal approach [36].

Usually, the petals forming the nanoflowers are 2D entities that arrange to form hierarchical three-dimensional (3D) morphologies. Thus, these hierarchical flower-like nanostructures can combine the advantages of 2D morphology along with the relatively higher dimensional 3D morphology. MoS_2 2D layers generally consist of a hexagonal layer of Mo atoms sandwiched between two layers of sulfur where the interlayer interaction is dominated by van der Waal's forces [1]. Usually, proper tuning of properties can and does play a critical role in various applications of MoS_2. For example, exfoliation of MoS_2 layers or limiting the bulk MoS_2 to a few layers tend to transform the indirect band-gap of MoS_2 to a direct one making them excellent semiconductor materials suitable for optoelectronic and nanoelectronics [6]. Tuning the morphology to adjust the ratio of edge sites with that of the surface sites also has important ramifications for these types of 2D layered materials in catalytic applications [2, 18, 37]. Thus, it is critical to evaluate the optimized conditions for maximizing the physicochemical characteristics required for specific application purposes. Detailed investigations into the synthesis parameters and their effects leading to the structural modifications are paramount.

In this work, we have synthesized flower-like MoS_2 via a simple hydrothermal method. We followed a previously reported synthesis template [28] and chose two different synthesis temperatures (200 °C and 220 °C) to observe its effects on various properties. These temperatures were picked due to previous literature suggesting the formation of well-defined flower-like MoS_2 around these regions. Higher temperatures were not chosen due to the practical limitations of the Teflon pots used during the hydrothermal treatment. The as-synthesized MoS_2 particles were crystallographically investigated by XRD and Raman spectroscopy and the effects of varying temperatures on grain size, crystallinity, etc. were evaluated. These properties hold particular importance for the effectiveness of the particles in electrocatalysis, sensing, or optoelectronics [37, 38]. We have generated 3D visualization of the crystal structures of the particles by applying the VESTA (visualization for electronic and structural analysis) software. Structural visualizations are important for creating databases and for initializing structures for various theoretical calculations. We have essentially studied the effect of temperature on various structural parameters; which would be useful for condition based-structure simulation. Effect on morphology and change in interlayer spacings were investigated by electron microscopic techniques. Again the change in spacings strongly influences its applicability in batteries due to enhanced capacity of metal insertion within the layers, and also in HER due to the electron hopping mechanism for layered materials [21, 37]. Effects on optical properties such as the bandgap of the particles were investigated by UV–vis spectroscopy. The nature and value of the bandgap both have important repercussions for MoS_2 being utilized as a semiconductor [25]. Overall, various facets of this paper discuss the effect of temperature variation on different properties of MoS_2 hierarchical flower-like particles, that dictate its performance in important applications.

2. Experimental details

2.1. Materials

Ammonium molybdate tetrahydrate ($(NH_4)_6Mo_7O_{24}.4H_2O$) with purity of 81–83% (MoO_3 basis) was purchased from Sigma-Aldrich Co. Ltd. Thiourea (CH_4N_2S) with purity of 99.9% (dried basis) was purchased

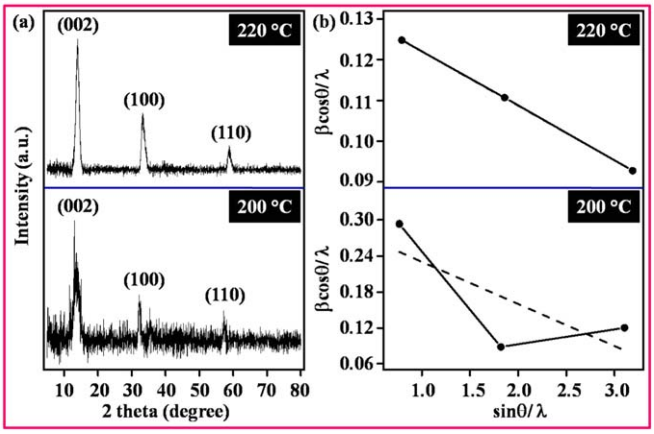

Figure 1. (a) X-ray diffraction patterns and (b) Williamson-Hall plots of MoS_2 nanoflowers synthesized via hydrothermal method at 200 °C (lower segment) and 220 °C (upper segment) for 6 h.

from Merck Life Science Pvt. Ltd. Absolute ethanol (C_2H_5OH) with purity of 99.9% was purchased from Changshu Hongsheng Fine Chemical Co. Ltd. All the materials used for the synthesis of MoS_2 hierarchical nanostructures were of Analytical Reagent (AR) grade and were used directly without any further purification. Millipore water (18 MΩ cm^{-1}) was used throuhout for the preparation of different solutions and further purification process.

2.2. Synthesis of MoS_2 nanoflowers

MoS_2 nanoflowers were fabricated by via a simple one-step hydrothermal method with varying temperatures using $(NH_4)_6Mo_7O_{24}.4H_2O$ and CH_4N_2S as starting materials. The hydrothermal synthetic methodology was performed with an optimized molar ratio 1:30 of Mo to S source materials. In a typical synthesis procedure, 0.028 M $(NH_4)_6Mo_7O_{24}.4H_2O$ and 0.84 M CH_4N_2S were dissolved in 36 ml of Millipore water under constant stirring at rom temperature to produce a transparent homogeneous solution. The above solution was stirred at 900 rpm for 1 h following which it was transferred to a 100 ml Teflon-lined stainless steel autoclave and sealed. The hydrothermal reaction was carried out in a hot air oven at two different temperatures of 200 and 220 °C for 6 h. The autoclave was then naturally cooled down to the room temperature. The resultant black precipitate was filtered out and washed several times with Millipore water and absolute ethanol repeatedly. Finally, the sample was collected and dried at 60 °C for 24 h. The different temperatures used in the synthesis process allowed us to observe the influence of synthesis temperature on the crystallographic and morphological properties of MoS_2.

2.3. Characterization of synthesized MoS_2 nanoflowers

The crystallographic characteristics of the as-synthesized samples were examined using powder XRD method (PAN analytical X'pert pro, Netherlands) with monochromatized Cu-$k_{\alpha 1}$ radiation ($\lambda = 1.54060$ Å), scanned between 2θ range of 5° to 80°. Raman spectra of the samples were rerecord on a confocal micro-Raman system UniRam) with an excitation source of 532 nm laser (15 mW power). The surface morphology of the samples was observed by a FESEM (Tescan Maia3). The structural model depicting a 3D crystallographic representation was achieved using the VESTA theoretical tool. The absorption spectra of the samples were investigated by a Double Beam UV–vis Spectrophotometer (Motra's UV Plus).

3. Results and discussion

3.1. Crystallographic identification

The basic crystallographic informations such as the crystal structure, crystallite size and purity of the as synthesized materials was evaluated by the XRD patterns. Figures 1(a)–(b) shows the XRD patterns and plots of $(\beta\cos\theta)/\lambda$ *versus* $(\sin\theta)/\lambda$ of the as prepared MoS_2 products. Figure 1(a) demonstrates the XRD pattern of the samples synthesized at 200 °C (lower segment) and 220 °C (upper segment). The identified peak positions at 13.55, 32.58 and 57.14° in the lower segment (200 °C); and 14.00, 33.28 and 58.83° in the upper segment (220 °C) and their relative intensities were in agreement respectively with the (002), (100) and (110) crystal planes of the hexagonal 2H-MoS_2 (standard JCPDS card no. 37–1492; space group P63/mmc, No. 194) [2, 6, 16, 22] with unit cell parameters of a = b = 3.16 Å and c = 12.29 Å; $\alpha = \beta = 90°, \gamma = 120°$. No peaks corresponding to any impurity and other phases of any material were observed indicating high purity and good

crystallinity of synthesized materials. The % yield obtained for the MoS_2 sample synthesized at 200 °C was determined to be 89.53% and for the MoS_2 sample synthesized at 220 °C it was 91.10%. The details of the calculation were provided in the supporting information (SI) (available online at stacks.iop.org/NANO/3/035001/mmedia). It was interesting to observe that the intensity of diffraction peaks became stronger and sharper with the increase of synthesis temperature suggesting improvement in crystallinity and increment of crystallite sizes. In XRD plots, the width of XRD peaks is considerably broadened at lower synthesis temperature, indicating small size of crystallites. The broadening is observed at 200 °C due to the smaller-sized nanocrystallites.

The strong intense (002) diffraction peak reveals that the material has a large number of crystal planes oriented in that particular direction and corresponds to the stacking of single layers of MoS_2 2D nanosheets [24, 31]. All the diffraction peaks shifted to a slightly higher angle with increasing synthesis temperature indicating lowered interplanar spacing (d-spacing). This phenomenon of decreased d-spacing with increasing synthesis temperature has also been previously observed [21, 39, 40]. We suggest the increased crystallite size of the particles to be the reason behind that. An increasing particle/crystallite size would increase the van-der waal's interaction between the layers and thus would bring them closer. Moreover, the ratio of d-spacing between the (100) and (110) lattice planes was estimated to be ~1.72, which is very close to $\sqrt{3}$:1, further authenticating the hexagonal structure of MoS_2 [41]. The estimated crystallite sizes from the Scherrer's relation [10] using the full width at half maxima (FWHM) values of the diffraction peaks obtained via their Gaussian fitting were within the range of 3–10 nm. Also, the dominant (002) peak observed in the XRD pattern of the 200 °C sample is relatively broad compared to the (002) peak observed in the XRD pattern observed of the 220 °C sample, which could also be attributed to the larger crystallite size of the former.

Figure 1(b) demonstrates the size-strain plot of $(\beta\cos\theta)/\lambda$ *versus* $(\sin\theta)/\lambda$ of the MoS_2 samples synthesized at 200 °C (lower segment) and 220 °C (upper segment). Generally, stress and strain almost always exist in the nanostructured materials (nanomaterials). Most of the cases, these stresses are residual stresses introduced into the system during the adopted synthesis process of nanomaterials. The positive value of strain indicates the tensile strain, whereas the negative value corresponds to the compressive strain of nanomaterials. Table 1 shows the summary of identified peak positions, relative intensities, corresponding lattice planes and calculated crystallite sizes using the FWHM obtained from the XRD patterns. In the present study, compressive strain was observed in both samples. Less compressive strain observed in the high temperature (220 °C) sample would indicate lesser deformation when compared to the low temperature (200°C) sample against applied stress. Thus from a mechanical strength related application viewpoint the MoS_2 (220) would be more suitable. Moreover, the average crystallite size (D_{av}) was also observed using Williamson-Hall method and its value was found to be ~3.32 nm and ~7.38 nm for the samples synthesized at 200 °C and 220 °C, respectively. The reason behind the larger crystallite size in the higher temperature sample can be understood by considering the phenomena of grain growth in the metallurgical processes where, with increasing temperature, the grain boundaries are removed and different crystallite zones are merged to form a larger crystallite [10].

The anisotropic properties including specific heat, tensile strength, dielectric strength, and electric as well as magnetic permeability of polycrystalline materials are related to the orientation distribution function of crystallites and its average value provides the orientation factor. The orientation factor signifies the process of orienting or the state of being oriented. The position or positioning in relation to the points of the compass or other specific directions is known as the orientation factor of any given state. The orientation factor is represented as O_{hkl}, where hkl is the orientation of planes, also known as the miller indices. For defining O_{hkl} mathematically, it requires the values of I_{std} and I_{exp} and a summation of their ratio, where I_{std} is assigned to the standard value of intensity and I_{exp} is the experimental value of the intensity. Mathematically, it is expressed by equation (1);

The orientation factors were calculated for the MoS_2 samples and were observed to be ranging between 18%–43% for 200 °C and 23%–45% for 220 °C synthesis temperature (table 2); suggesting that the anisotropic properties enhanced with increasing synthesis temperatures.

$$O_{hkl}(\%) = \frac{I_{\exp}/I_{std}}{\sum(I_{\exp}/I_{std})} \times 100 \quad (1)$$

Further insights into the phase formation of the MoS_2 particles can be obtained by examining their lattice vibrations (phonons), and Raman spectroscopy was performed for this purpose. Raman spectra of the MoS_2 samples synthesized at two different temperatures are put up in figure 2. Both the samples contained three distinct Raman peaks at 147, 194, and 237 cm^{-1}, which can be attributed to the presence of elemental sulfur [22]. One intense peak was observed at 281 cm^{-1} (E_{1g}; in-plane symmetric stretching of terminal atoms), characteristic of hexagonal MoS_2 [19, 24]. The other two peaks appearing at 374 and 413 cm^{-1} reveal first-order Raman vibration modes E^1_{2g} (in-plane opposite vibrations of Mo/S atoms) and A_{1g} (out-of-plane of S atoms), respectively, within the S-Mo-S layer of hexagonal MoS_2 [24, 26, 32]. The Raman peak at 464 cm^{-1} is assigned to

Table 1. A summary of identified peak position (2θ value) and relative intensity with crystallite size for MoS_2 nanoflowers.

Synthesis temperature	2theta (degree)	Intensity (a. u.)	Interplaner spacing (d nm)	Lattice plane (h k l)	FWHM (β degree)	Crystallite size (D nm)	Average crystallite size (D_{av})	Strain value (type)
200 °C	13.55	193.56	0.653	(0 0 2)	2.61	3.03	3.32 nm	− 0.0705 (compressive)
	32.58	90.00	0.274	(1 0 0)	0.81	10.11		
	57.14	65.66	0.161	(1 1 0)	1.21	7.39		
220 °C	14.00	1088.45	0.632	(0 0 2)	1.11	7.13	7.38 nm	− 0.0133 (compressive)
	33.28	476.82	0.269	(1 0 0)	1.02	8.04		
	58.83	204.33	0.156	(1 1 0)	0.94	9.60		

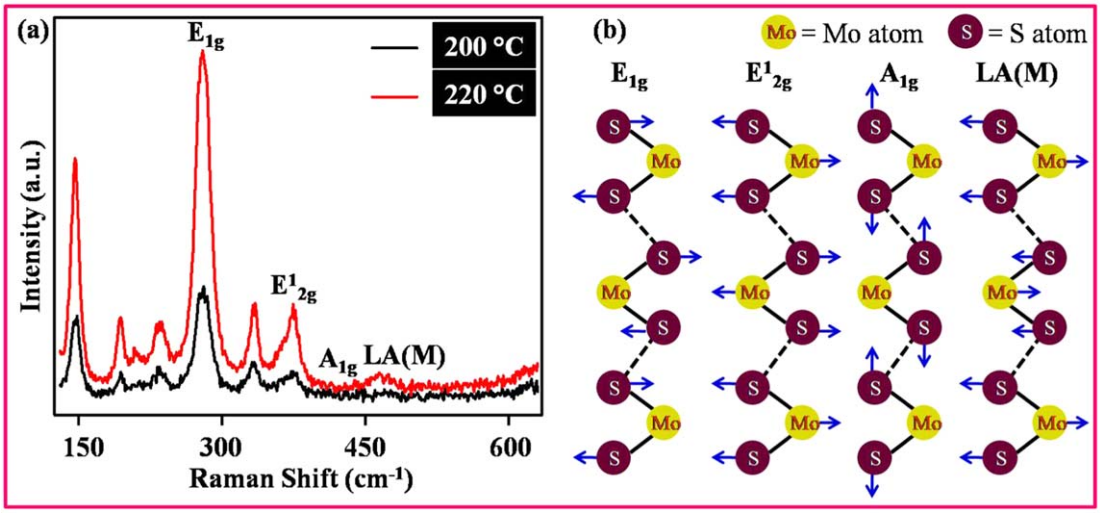

Figure 2. (a) Raman spectra of MoS_2 nanoflowers synthesized via hydrothermal method at two different temperatures and (b) Schematic illustrations of typical Raman-active phonon modes (E_{1g}, E^1_{2g}, A_{1g} and LA(M)).

Table 2. An overview of orientation factor obtained from XRD analysis for MoS_2 nanoflowers obtained at two different synthesis temperatures.

Synthesis temperature	Lattice plane (h k l)	I_{exp}	I_{std}	O_{hkl} (%)
200 °C	(0 0 2)	193.56	100	18.06
	(1 0 0)	90.00	22	38.17
	(1 1 0)	65.66	14	43.76
220 °C	(0 0 2)	1088.45	100	23.08
	(1 0 0)	476.82	22	45.96
	(1 1 0)	204.33	14	30.95

the secondary phonon mode (longitudinal acoustic mode at M point; LA(M)) [24]. With the increasing hydrothermal temperature, the intensity of all Raman peaks becomes sharper and more intense, revealing enhancement of crystalline quality and reduction of structural defect states, which is in accordance with the results obtained from XRD [21, 24]. The relatively larger FWHM values and weaker intensity of the E^1_{2g} peak can be attributed to the phonon confinement and also indicates that the crystal structures include substantial defect sites [19, 21, 24]. Moreover, the intensity of E^1_{2g} peak is higher than that of A_{1g}, indicating that the synthesized MoS_2 samples have strong in-plane opposite vibrations, which suggests that the edges of MoS_2 nano-flowers are highly exposed [26, 32]. The schematic illustrations of different Raman phonon modes are depicted in figure 2(b) elucidating the displacement of Mo and S atoms in diverse vibrating modes.

3.2. Morphology analysis

The surface morphology of the particles was examined by FESEM and a flower-like round hierarchical morphology was quite evident across both sets of particles corresponding to different synthesis temperatures. Figures 3(a)–(b) elucidates the low and high magnification FESEM images of MoS_2 nanoflowers synthesized at 200 °C. From the low magnification FESEM image (figure 3(a)), it is clearly visible that the MoS_2 sample is composed of highly dense and uniform agglomerated 3D flower-like hierarchical structures. The dimension of these structures on average is closer to 500 ($\pm$10) nm in diameter. The high magnification FESEM image (2b), reveals that the MoS_2 nanoflowers consist of ultrathin nanoplatelets of about 15 ($\pm$3) nm in thickness (the thickness of individual platelets is marked by yellow arrows and marked as symbol B). These nanoplatelets show a tendency for agglomeration to form 3D flower-like morphology (denoted by blue encircled area A). In these nanoflowers, some platelets randomly situate in the center of the overall flower whereas some platelets intersect with each other. Figures 3(c)–(d) displays the low and high magnification FESEM images of MoS_2 hierarchical nanostructures obtained at 220 °C. Figure 3(c) provides the low-magnification FESEM image portraying 3D flower-like hierarchical MoS_2 nanoparticles with high uniformity. The estimated sizes of these MoS_2 flower-like

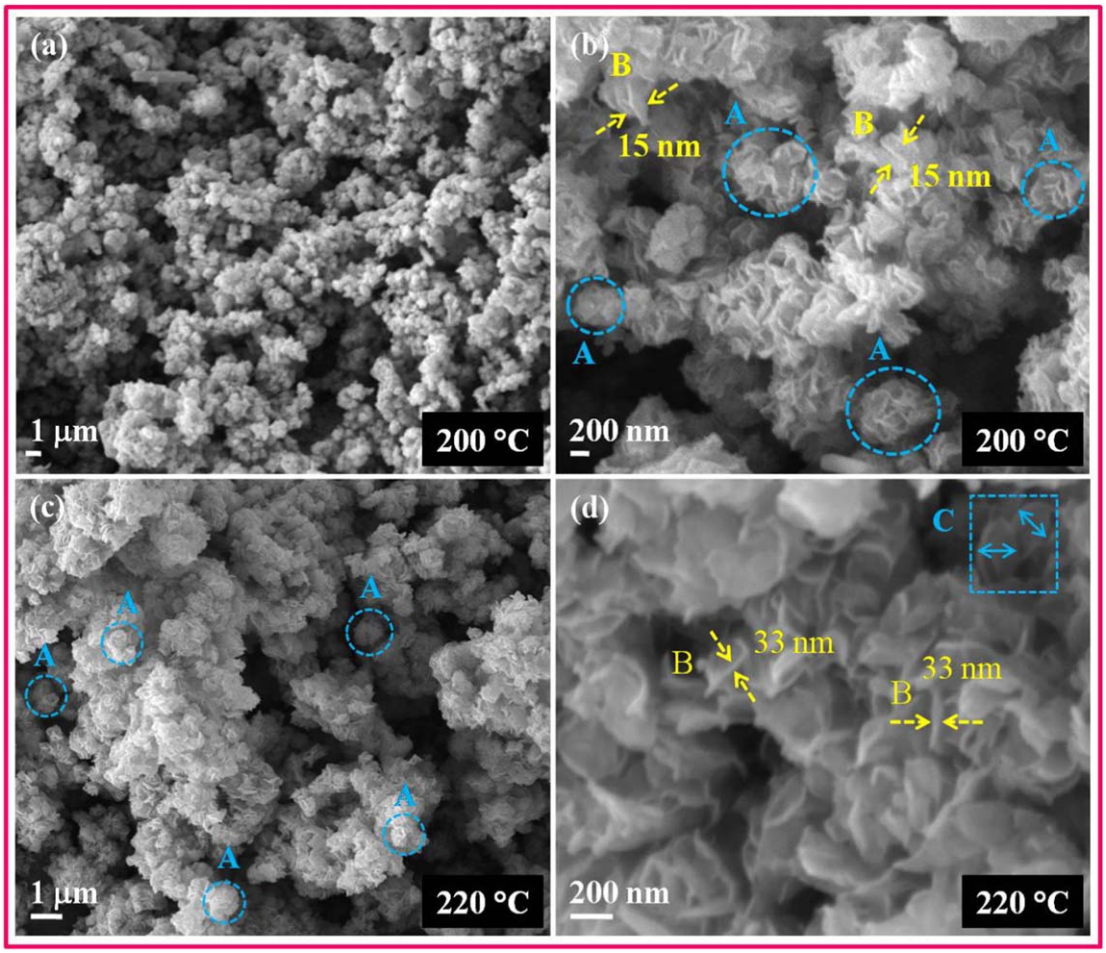

Figure 3. FESEM images at different magnifications; (a, c) low magnification and (b, d) high magnification of MoS_2 nanoflowers synthesized via hydrothermal method at two different temperatures (200 °C, 220 °C) for 6 h.

structures were apparently in the range of ~500–700 (±15) nm on average. It is obvious that the morphology of the flower-like grains is uniform in each region (as represented by the blue dotted circles and marked with symbol A in figure 3(c)). Figure 3(d) elucidates the high magnification FESEM image revealing that the MoS_2 nanoflowers are made up of numerous stacked 2D nanosheets (nanoplatelets) having diameters in the range of 150–180 (±5) nm (as indicated by the blue arrows in the blue dotted rectangle marked by 'C' in figure 3(d)). The thickness of the platelets was in the range of 30–35 nm (the thickness of an individual nanoplatelet is marked by yellow arrows and indicated as symbol B in figure 3(d)). These nanoplatelets were attached to each other to produce the 3D flower-like hierarchical nanostructure of MoS_2 crystals. The morphology of the particles in all their regions is uniform (as represented by blue dotted circles). The average thickness of the platelets and the overall size of the MoS_2 flowers increase with increasing synthesis temperature as was evident from figure 3, signifying enhanced growth post nucleation and improved morphological quality. Moreover, the surface morphology of the hierarchical nanostructures reported in this article resembles to the typical nanoflower morphology reported previously for the hydrothermal synthesis of MoS_2 [18, 19, 21, 24, 32]. The rounded flower-like morphology assembled by nanoplatelets of MoS_2 hierarchical nanostructures suggesting more effective sensing performances for easy distribution of interacting surfaces.

3.3. Crystallography visualization perspective

Figure 4 displays the 3D wireframe structure model with individual crystal planes, as observed in the XRD pattern of hierarchical MoS_2 nanostructures. From figure 4(a), it can be observed that the crystallographic sites for Mo and S atoms are in the hexagonal unit cell of MoS_2 crystal structure. Moreover, each Mo atom is attached to four S atoms (two S1 and two S2 atoms) and each S atom is shared by two Mo atoms, leading to the formation of hexagonal MoS_2 structure. In a hexagonal MoS_2 crystal structure, each Mo atom is trigonal prismatically coordinated with the nearby S atoms. The simulated interatomic distances of Mo and S atoms in MoS_2 structure

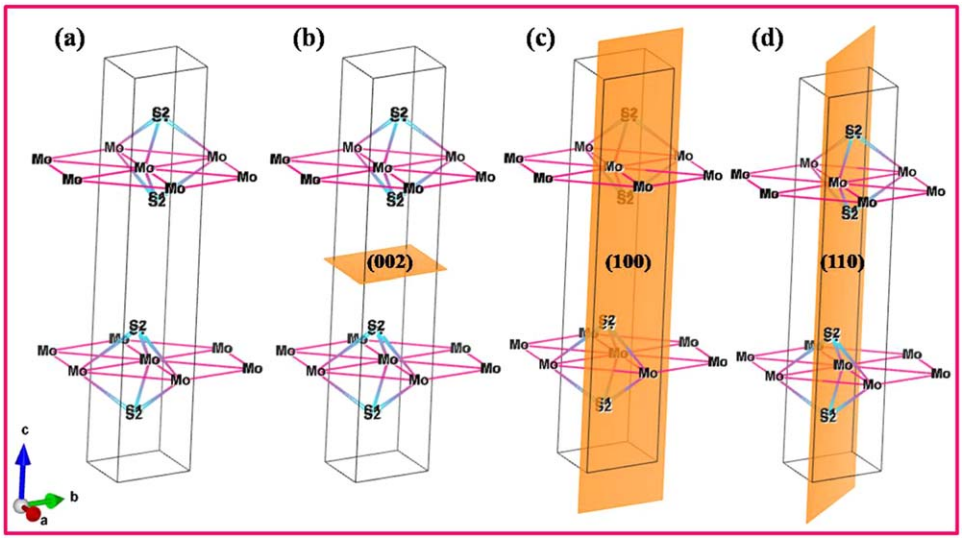

Figure 4. 3D crystallographic representation of (a) wireframe structure model, and (b)-(d) structure model associated with individual lattice plane: (b) (002), (c) (100) and (d) (110) planes as observed in XRD pattern of hexagonal MoS_2. Color code: slices in Orange color represents the corresponding lattice plane.

Table 3. Theoretical interatomic distance obtained by VESTA tool for MoS_2 structure.

Atoms		Interatomic distance
Atom 1	Atom 2	(Å)
Mo	Mo	3.162
Mo	S1	2.186
Mo	S2	2.258

obtained by employing the VESTA theoretical tool are provided in table 3. The observed crystal planes in XRD pattern, (002), (100), and (110) are displayed in figures 4(b), (c) and (d), respectively.

3.4. Growth mechanism of MoS_2 nanoflowers

Based on the crystallographic and morphological analysis, the plausible growth mechanism of MoS_2 nanoflowers consisting of stacked 2D nanosheets (nanoplatelets) is proposed as illustrated schematically in figure 5. In this synthesis process, the growth mechanism consists of three stages; (i) rapid nucleation, (ii) oriented aggregation and (iii) self-assembly. Firstly, water containing $(NH_4)_6Mo_7O_{24}.4H_2O$ and CH_4N_2S as respectively Mo^{4+} and S^{2-} sources collide elastically with each other at room temperature and form a transparent homogeneous solution. The synthesis of MoS_2 nanoflowers is carried out at the temperatures of 200/220 °C, which lies between the boiling point and critical temperature of water. In hydrothermal treatment, the hydrolysis of CH_4N_2S to H_2S gas begins to create high pressure leading to the formation of MoS_2 nuclei which grow into S-Mo-S layers. Subsequently, the growth of nanosheets takes place during oriented aggregation of primary nuclei due to high stress. These nanosheets act as core to initiate the formation of nanoflowers through self-assembly process. The driving force behind the peculiar hierarchical disposition may be any one of the factors including van der Waals forces, ionic interactions, hydrogen bonds, hydrophobic interactions, and synergistic parameters. Furthermore, as the hydrothermal temperature is increased, the nucleation process becomes more dominant resulting in favor of increasing sizes, and the quality of crystals of MoS_2 nanoflowers, as observed in the crystallography and morphology analysis.

3.5. Optical properties

It is well known that an optical transition (absorption and/or emission) occurs when a photon is absorbed or emitted by the defect states [42, 43]. Therefore, in order to correlate the optical properties with crystallography and morphology analysis of MoS_2, UV–vis spectroscopy was carried out using an aqueous dispersion of the MoS_2 particles. Figure 6(a) depicts UV–vis absorption spectra of MoS_2 samples synthesized at two different temperatures. Both MoS_2 samples reveal broad absorption within 300 to 700 nm. The obtained UV–vis

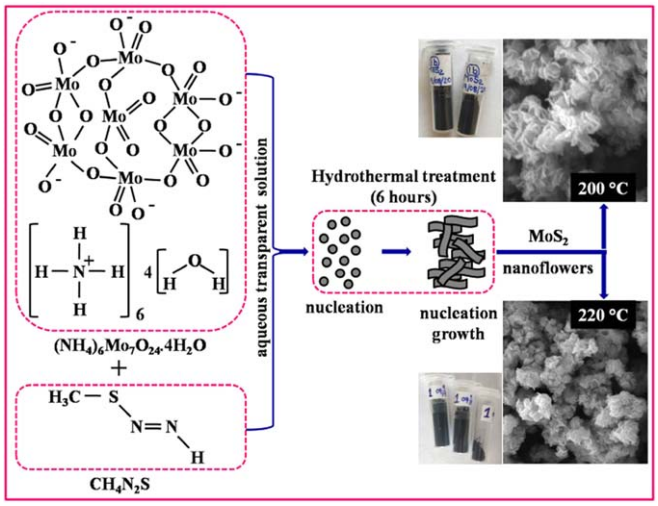

Figure 5. Schematic illustration for the plausible growth mechanism of 3D MoS_2 hierarchical nanoflowers assembled by stacked 2D nanosheets synthesized via hydrothermal method with varying temperatures.

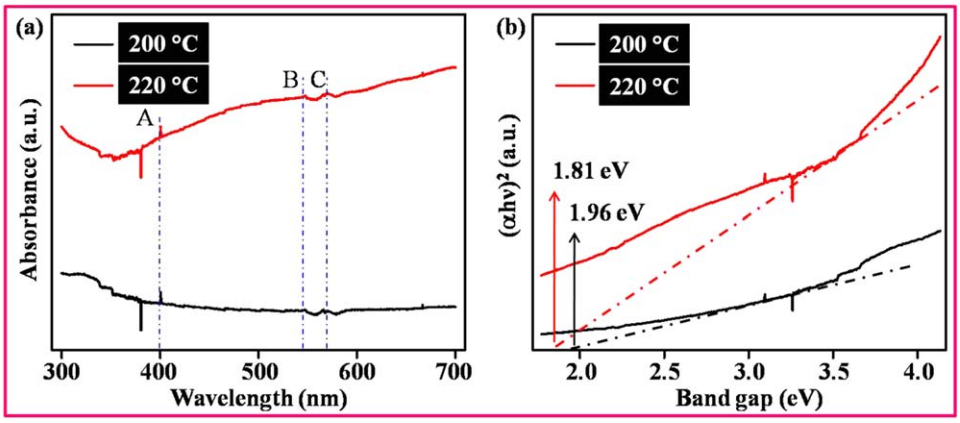

Figure 6. (a) UV–vis absorption spectra and (b) Tauc plots for assessing optical band gap of MoS_2 nanoflowers synthesized via hydrothermal method at two different temperatures (200 °C, 220 °C) for 6 h.

absorption spectra elucidate three excitons; exciton A at 400 nm (3.1 eV), exciton B at 547 nm (2.26 eV), and exciton C at 570 nm (2.17 eV) (as indicated by blue dotted lines in figure 6(a)), due to the electronic transitions at energy levels indicating the adsorption sites are different [43–45]. Excitonic peaks observed at lower wavelength and higher wavelength regions signify the indirect to direct band transition at the edge of the Brillouin zone and quantum confinement phenomenon, respectively [10, 28]. The corresponding optical band gaps (E_g) are evaluated from UV–vis spectra by using the Tauc equation (2);

$$(\alpha h\nu)^{n} = A(h\nu - E_g) \tag{2}$$

Where α is the absorption coefficient obtained using Beer–Lambert law, $h\nu$ is the energy of the incident photon, n is 2 or ½ for direct or indirect bandgap transition and A is characteristic of material with constant value [10, 42].

Figure 6(b) displays the intercept on the abscissa of the plot of $(\alpha h\nu)^2$ against photon energy $h\nu$ revealing the bandgap energy of the samples. The corresponding bandgap for the MoS_2 sample synthesized at 200 °C was calculated to be 1.96 eV and it was 1.81 eV for the MoS_2 sample at 220 °C. The obtained result agreed well with the reported band gap values for MoS_2 hierarchical nanostructures ranging between 1.58–2.32 eV [27, 29, 30]. The higher band gap value of MoS_2 sample synthesized at a lower temperature could be assigned to the small crystallite size and particle size of its nanoparticles which could be resulting in a quantum confinement effect [10, 46]. No obvious linear relation was established for $n = ½$ demonstrating the absence of any indirect band gap in the MoS_2 samples.

4. Conclusions

In summary, 3D MoS_2 hierarchical nanoflowers consisting of stacked 2D nanoplatelets were successfully synthesized by a facile hydrothermal method at two different temperatures, using $(NH_4)_6Mo_7O_{24}.4H_2O$ and CH_4N_2S as starting materials. A significant change is reflected in crystallography and morphology characteristics of nanostructures with varying the synthesis temperature. The XRD patterns revealed that the synthesized MoS_2 hierarchical nanoflowers are well crystallized and both crystallinity and crystallite sizes enhance with increasing temperature. FESEM micrographs revealed that both of the as-synthesized materials possessed uniform hierarchical rounded 3D flower-like morphology composed of nanoplatelets which were basically stacked ultrathin 2D nanosheets. Increasing the hydrothermal temperature increases the thickness of the platelets by almost twice. Visualization of the corresponding crystal structures via 3D wireframe structure model associated with different lattice planes has been carried out from a crystallographic perspective. The bandgap of the materials was observed to decrease with increased hydrothermal temperature indicating the synthesis temperature has implications for the application of the material as a semiconductor. A plausible growth mechanism for the formation of MoS_2 nanoflowers has been proposed, which is correlated with experimental observations and analysis. We believe that the findings in this paper will have a considerable impact while analyzing its fabrication condition-based properties which would be critical in different range of applications.

Acknowledgments

We would like to acknowledge the financial support from SERB-DST (ECR/2017/000879; Diary No./Finance No. SERB/F/7840/2018–2019). One of the authors, Kajal Kumar Dey would like to acknowledge the financial support received from VBS Purvanchal University (Letter No. 133/Purvanchal University/IQAC/2022 dt. 23/03/2022). Authors would like to express their gratitude to Central Facilities for Materials Characterization, Prof. Rajendra Singh (Rajju Bhaiya) Institute of Physical Sciences for Study and Research, VBS Purvanchal University, Jaunpur for providing FESEM and UV–vis facility. We also thank Prof. K N Uttam, Deprtment of Physics, University of Allahabad, for providing the Raman spectroscopy facility.

Data availability statement

All data that support the findings of this study are included within the article (and any supplementary files).

ORCID iDs

Kajal Kumar Dey https://orcid.org/0000-0001-8930-6708
Jitendra Gangwar https://orcid.org/0000-0002-1527-9601

References

[1] Coleman J N *et al* 2011 Two-dimensional nanosheets produced by liquid exfoliation of layered materials *Science* **331** 568–71
[2] Kong D, Wang H, Cha J J, Pasta M, Koski K J, Yao J and Cui Y 2013 Synthesis of MoS_2 and $MoSe_2$ films with vertically aligned layers *Nano Lett.* **13** 1341–7
[3] Rani A, Dhiman R L, Singh V, Kumar S and Kumar S 2021 Photocatalytic study of Ni-N-codoped TiO_2 nanoparticles under visible light irradiation *Nano Express* **2** 030002
[4] Kumar N, Bahl T and Kumar R 2020 Study of the methylene blue adsorption mechanism using ZrO_2/Polyaniline nanocomposite *Nano Express* **1** 030025
[5] Singh Neetu, Kumar N D and Gangwar J 2019 Comparative study of crystallographic representation on the three ZrO_2 polymorphs: structural models, lattice planes, model electron and nuclear densities *Mater. Res. Express* **6** 150f8
[6] Yin X, Ye Z, Chenet D A, Ye Y, O'Brien K, Hone J C and Zhang X 2014 Edge nonlinear optics on a MoS_2 atomic monolayer *Science* **344** 488–90
[7] Jungclaus J, Spende H, Hille P, Schörmann J, Waag A, Eickhoff M and Voss T 2021 Time-resolved cathodoluminescence investigations of AlN:Ge/GaN nanowire structures *Nano Express* **2** 034001
[8] Gangwar J, Gupta B K, Tripathi S K and Srivastava A K 2015 Phase dependent thermal and spectroscopic responses of Al_2O_3 nanostructures with different morphogenesis *Nanoscale* **7** 13313–44
[9] Kondo D, Kataoka M, Hayashi K and Sato S 2021 Few-layer hexagonal boron nitride synthesized by chemical vapor deposition and its insulating properties *Nano Express* **2** 030001
[10] Gangwar J, Dey K K, Tripathi S K, Wan M, Yadav R R, Singh R K, Samta and Srivastava A K 2013 NiO-based nanostructures with efficient optical and electrochemical properties for high-performance nanofluids *Nanotechnology* **24** 415705
[11] Nasalapure A V, Chalannavar R K, Kasai D R, Reddy K R and Raghu A V 2021 Novel polymeric hydrogel composites: Synthesis, physicochemical, mechanical and biocompatible properties *Nano Express* **2** 030003
[12] Masuzawa T, Okigawa Y, Ogawa S, Takakuwa Y, Hatakeyama K and Yamada T 2021 Synthesis and characterization of potassium-doped multilayer graphene prepared by wet process using potassium hydroxide *Nano Express* **2** 030004

[13] Nath M, Govindaraj A and Rao C N R 2001 Simple Synthesis of MoS_2 and WS_2 Nanotubes *Adv. Mater.* **13** 283–6
[14] Yu Y *et al* 2018 High phase-purity 1T′-MoS_2- and 1T′-$MoSe_2$-layered crystals *Nat. Chem.* **10** 638–43
[15] Zhao W, Pan J, Fang Y, Che X, Wang D, Bu K and Huang F 2018 Metastable MoS_2: crystal structure, electronic band structure, synthetic approach and intriguing physical properties *Chem. Eur. J.* **24** 15942–54
[16] Hu Z, Wang L, Zhang K, Wang J, Cheng F, Tao Z and Chen J 2014 MoS_2 nanoflowers with expanded interlayers as high-performance *Angew. Chem. Int. Ed.* **53** 12794–8
[17] Lin Z *et al* 2018 Solution-processable 2D semiconductors for high performance large-area electronics *Nature* **562** 254–8
[18] He Z and Que W 2016 Molybdenum disulfide nanomaterials: Structures, properties, synthesis and recent progress on hydrogen evolution reaction Appl *Mater. Today* **3** 23–56
[19] Deokar G, Vignaud D, Arenal R, Louette P and Colomer J F 2016 Synthesis and characterization of MoS_2 nanosheets *Nanotechnology* **27** 075604
[20] Park S, Lee A, Choi K H, Hyeong S K, Bae S, Hong J M, Kim T W, Hong B H and Lee S K 2020 Layer-selective synthesis of MoS_2 and WS_2 structures under ambient conditions for customized electronics *ACS Nano* **14** 8485–94
[21] Lu Y, Yao X, Yin J, Peng G, Cui P and Xu X 2015 MoS_2 nanoflowers consisting of nanosheets with a controllable interlayer distance as high performance lithium ion battery anodes *RSC Adv.* **5** 7938–43
[22] Xu Z, Fu H, Yao K, Shen X, Li Z, Fu L, Huang J and Li J 2018 Elemental sulfur nanoparticles chemically boost the sodium storage performance of MoS_2/rGO anodes *Batter Supercaps* **1** 184–91
[23] Jaramillo T F, Jørgensen K P, Bonde J, Nielsen J H, Horch S and Chorkendorff I 2007 Identification of active edge sites for electrochemical H_2 evolution from MoS_2 nanocatalysts *Science* **317** 100–2
[24] Wang D, Pan Z, Wu Z, Wang Z and Liu Z 2014 Hydrothermal synthesis of MoS_2 nanoflowers as highly efficient hydrogen evolution reaction catalysts *J. Power Sources* **264** 229–34
[25] Huang Y L *et al* 2015 Bandgap tunability at single-layer molybdenum disulphide grain boundaries *Nat. Commun.* **6** 6298
[26] Lalithambika K C, Shanmugapriya K and Sriram S 2019 Photocatalytic activity of MoS_2 nanoparticles: an experimental and DFT analysis *Appl. Phys. A: Mater. Sci. Process.* **125** 817
[27] Singh J, Rishikesh, Kumar S and Soni R K 2020 Synthesis of 3D-MoS_2 nanoflowers with tunable surface area for the application in photocatalysis and SERS based sensing *J. Alloys Compd.* **849** 156502
[28] Thangudu S, Lee M T and Rtimi S 2020 Tandem synthesis of high yield MoS_2 nanosheets and enzyme peroxidase mimicking properties *Catalysts* **10** 1009
[29] Qumar U, Ikram M, Imran M, Haider A, Hamid A U, Haider J, Riaz K N and Ali S 2020 Synergetic effect of Bi-doped exfoliated MoS_2 nanosheets on its bactericidal and dye degradation potential *Dalton Trans.* **49** 5362–77
[30] He G, Zhnag Y and He Q 2019 MoS_2/CdS Heterostructure for enhanced photoelectrochemical performance under visible light *Catalysts* **9** 379
[31] Mani N P, Ganiga M and Cyriac J 2017 Synthesis of MoS_2 quantum dots uniformly dispersed on low dimensional MoS_2 nanosheets and unravelling its multiple emissive states *ChemistrySelect* **2** 5942–9
[32] Phuc N H H, Okuno T, Hakiri N, Kawamura G, Matsuda A and Muto H 2014 Synthesis of high-edge exposure MoS_2 nano flakes *J. Nanopart. Res.* **16** 2199
[33] Li M, Wang D, Li J, Pan Z, Ma H, Jiang Y and Tian Z 2016 Facile hydrothermal synthesis of MoS_2 nano-sheets with controllable structures and enhanced catalytic performance for anthracene hydrogenation *RSC Adv.* **6** 71534–42
[34] Ye L, Xu H, Zhang D and Chen S 2014 Synthesis of bilayer MoS_2 nanosheets by a facile hydrothermal method and their methyl orange adsorption capacity *Mater. Res. Bull.* **55** 221–8
[35] Arunbalaji S, Ismail M A M, Arivanandhan M, Alsalme A, Alghamdi A and Jayavel R 2020 High sensitive electrochemical nitrite sensor using Fe_2O_3/MoS_2 nanocomposites synthesized by facile method *Bull. Chem. Soc. Jpn.* **93** 1564–70
[36] Zhang X, Huang X, Xue M, Ye X, Lei W, Tang H and Li C 2015 Hydrothermal synthesis and characterization of 3D flower-like MoS_2 microspheres *Mater. Lett.* **148** 67–70
[37] Dey K K, Jha S, Kumar K, Gupta G, Srivastava A K and Ingole P P 2019 Layered vanadium oxide nanofibers as impressive electrocatalyst for hydrogen evolution reaction in acidic medium *Electrochim. Acta* **312** 89–99
[38] Yadav N, Chaudhary P, Dey K K, Yadav S, Yadav B C and Yadav R R 2020 Non-functionalized Au nanoparticles can act as high-performing humidity sensor *J. Mater. Sci., Mater. Electron.* **31** 17843–54
[39] Manzoor U, Siddique S, Ahmed R, Noreen Z, Bokhari H and Ahmad I 2016 Antibacterial, structural and optical characterization of mechano-chemically prepared ZnO nanoparticles *PLoS One* **11** e0154704
[40] Li N, Chai Y, Li Y, Tang Z, Dong B, Liu Y and Liu C 2012 Ionic liquid assisted hydrothermal synthesis of hollow vesicle-like MoS_2 microspheres *Mater. Lett.* **66** 236–8
[41] Zou X, Hovmöller S and Oleynikov P 2011 Electron crystallography: electron microscopy and electron diffraction *Oxford Science Publications* **16** 441
[42] Verma R, Naik K K, Gangwar J and Srivastava A K 2014 Morphology, mechanism and optical properties of nanometer-sized MgO synthesized via facile wet chemical method *Mater. Chem. Phys.* **148** 1064–70
[43] Kim H J, Song Y W, Namgung S D, Song M K, Yang S and Kwon J Y 2018 Optical properties of the crumpled pattern of selectively layered MoS_2 *Opt. Lett.* **43** 4590–3
[44] Gangwar J, Gupta B K, Kumar P, Tripathi S K and Srivastava A K 2014 Time-resolved and photoluminescence spectroscopy of θ-Al_2O_3 nanowires for promising fast optical sensor applications *Dalton Trans.* **43** 17034–43
[45] Gangwar J, Chandran A, Joshi T, Verma R, Biradar A M, Tripathi S K, Gupta B K and Srivastava A K 2015 *Mater. Res. Express* **2** 075013
[46] Gangwar J, Kim J, Kumar A, Bhatnagar D, Senthil K, Tripathi S K, Yong K and Srivastava A K 2013 Optimization control on growth morphology, lattice scale features and optical response of Al-incorporated ZnO nano-needles *Nanosci. Nanotechnol. Lett.* **5** 67–72